Phase transitions of single polymer chains and of polymer solutions: insights from Monte Carlo simulations

2008 J. Phys.: Condens. Matter 20 494215

(http://iopscience.iop.org/0953-8984/20/49/494215)

J. Phys.: Condens. Matter **20** (2008) 494215 (8pp) doi:10.1088/0953-8984/20/49/494215

Phase transitions of single polymer chains and of polymer solutions: insights from Monte Carlo simulations

K Binder[1], W Paul[1], T Strauch[1], F Rampf[1], V Ivanov[2] and J Luettmer-Strathmann[3,4]

[1] Institut für Physik, Johannes-Gutenberg-Universität, Staudinger Weg 7, D-55099 Mainz, Germany
[2] Faculty of Physics, Moscow State University, Moscow 119992, Russia
[3] Department of Physics, University of Akron, Akron, OH 44325-4001, USA
[4] Department of Chemistry, University of Akron, Akron, OH 44325-4001, USA

E-mail: kurt.binder@uni-mainz.de

Received 16 July 2008
Published 12 November 2008
Online at stacks.iop.org/JPhysCM/20/494215

Abstract

The statistical mechanics of flexible and semiflexible macromolecules is distinct from that of small molecule systems, since the thermodynamic limit can also be approached when the number of (effective) monomers of a single chain (realizable by a polymer solution in the dilute limit) is approaching infinity. One can introduce effective attractive interactions into a simulation model for a single chain such that a swollen coil contracts when the temperature is reduced, until excluded volume interactions are effectively canceled by attractive forces, and the chain conformation becomes almost Gaussian at the theta point. This state corresponds to a tricritical point, as the renormalization group theory shows. Below the theta temperature a fluid globule is predicted (at nonzero concentration then phase separation between dilute and semidilute solutions occurs), while at still lower temperature a transition to a solid phase (crystal or glass) occurs.

Monte Carlo simulations have shown, however, that the fluid globule phase may become suppressed, when the range of the effective attractive forces becomes too short, with the result that a direct (ultimately first-order) transition from the swollen coil to the solid occurs. This behavior is analogous to the behavior of colloidal particles with a very short range of attractive forces, where liquid–vapor-type phase separation may be suppressed. Analogous first-order transitions from swollen coils to dense rodlike or toroidal structures occur for semiflexible polymers. Finally, the modifications of the behavior discussed when the polymers are adsorbed at surfaces are also mentioned, and possible relations to wetting behavior of polymer solutions are addressed.

1. Introduction and overview

One of the most elementary problems of polymer physics is the behavior of very long flexible polymer chains in dilute solution when the solvent quality is varied [1, 2]. For simplicity, we assume solvent quality is controlled by varying the temperature T: at high T ($T > \Theta$) one has good solvent conditions, the gyration radius R_g of a chain scales with the number N of (effective) monomers like a self-avoiding walk (SAW), $R_g \propto N^{\nu}$ with [1, 2] $\nu \approx 0.59$, while at the so-called 'theta temperature' $T = \Theta$ one has random-walk (RW) type behavior, $R_g \propto N^{1/2}$. The idea is, that the short range repulsive interactions among the monomers (excluded volume!) that lead to the swelling of the random coil in the good solvent regime at $T = \Theta$ are effectively canceled by the attractive part of the forces (which has a somewhat longer range). For $T < \Theta$, however, these attractive forces 'win' and cause a 'collapse' of the coil to a globule which has a finite density ρ, (figure 1) $R_g \propto N^{1/3}$ and hence $\rho \propto N/R_g^3 \to \rho_{\text{liquid}} \neq 0$ as $N \to \infty$ (while $\rho \to 0$ for $N \to \infty$ if $T \geqslant \Theta$).

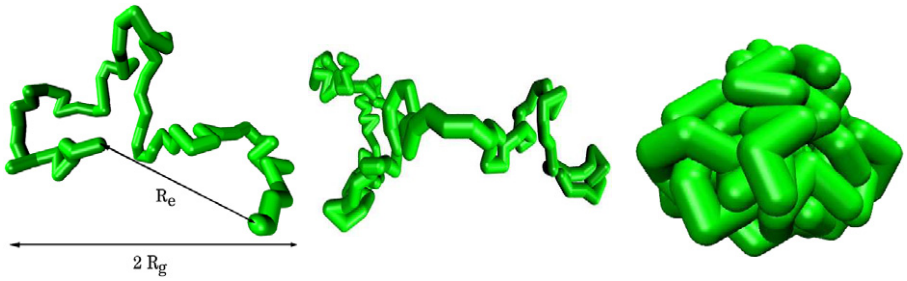

Figure 1. Snapshot pictures of a polymer coil, generated by Monte Carlo simulation of the bond fluctuation model (see section 2) on the simple cubic lattice, for $T \to \infty$ (left), $T = \Theta$ (middle) and $T \ll \Theta$ (right), for $N = 64$.
(This figure is in colour only in the electronic version)

This behavior is easily understood on a mean-field level, considering the second virial coefficient $B(T)$ [2]

$$B(T) = \tfrac{1}{2} \int (1 - \exp[-U(\vec{r})/T])\, \mathrm{d}^3\vec{r}, \qquad (1)$$

where $U(\vec{r})$ is the interaction potential between the monomers. In dilute solution, the osmotic equation of state can be written in terms of the virial expansion (n = number of polymers per unit volume; $p_{\mathrm{id}} = nT$ is the ideal gas contribution)

$$p_{\mathrm{osm}}(T) = p(n, T) - nT = nB(T) + 2n^2C(T) + \cdots, \quad (2)$$

where $C(T)$ is the third virial coefficient. Now in mean-field theory $B(T)$ changes sign at $T = \Theta$, $B(T) = b\tau$ with $\tau = (T - \Theta)/\Theta$, and hence for $T < \Theta$ there exists a solution with $p_{\mathrm{osm}}(n_0, T) = 0$ with $n_0 = -B/(2C) \propto (\Theta - T) > 0$. Since $n_0 \to 0$ when Θ is approached from below, close to $T = \Theta$ the use of the virial equation of state is self-consistent.

Nevertheless the picture changes slightly when renormalization group theory is invoked [1–3]. The Θ-point takes then the character of a tricritical point, and the relation $R_{\mathrm{g}} \propto N^{1/2}$ is modified by logarithmic corrections. In addition, the Θ point no longer is given by $B(T = \Theta) = 0$ but one has to consider the variation of the (scale-dependent) virial coefficient $B_{\mathrm{s}}(T)$ under transformation of the scale s along the chain: $T = \Theta$ then is found when the renormalized virial coefficient $\beta(T) = B_\infty(T)$ vanishes, while for $T > \Theta$ all renormalization group trajectories end up at a nonzero fixed point value β^* independent of T for $T > \Theta$, reflecting universal behavior (the exponent ν does not depend on T).

While this standard picture, as sketched above, is widely accepted as the standard wisdom, experimental evidence for some crucial aspects still is almost completely lacking: so far the theoretically predicted logarithmic corrections have not yet been clearly identified, and experimental studies of the collapsed globular state of single polymer coils are hampered by hysteresis effects [4]. Simulation studies saw some logarithmic corrections at $T = \Theta$, but not in accord with the theory [5].

In the present paper, we reconsider this problem and shall point out that the scenario sketched in figure 1 is incomplete because it disregards other states of a single polymer chain that may compete with those shown. It has already been known since a long time [6–8] that local chain stiffness is a relevant parameter: so the coil-globule transition may be replaced by

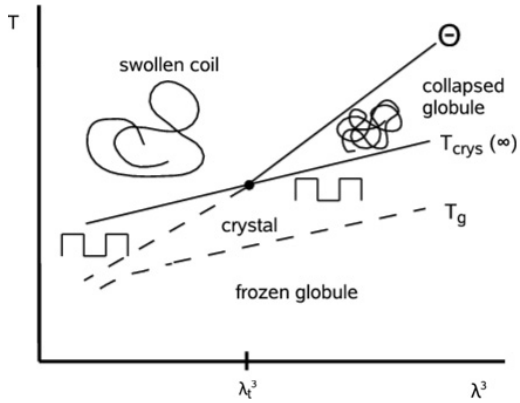

Figure 2. Schematic phase diagram of a single flexible polymer chain in the thermodynamic limit ($N \to \infty$) as a function of temperature T and range of attractive monomer–monomer interaction λ. For $\lambda > \lambda_t$ there occurs a transition at $T = \Theta$ from the swollen coil to the collapsed globule and at $T_{\mathrm{crys}}(\infty) < \Theta$ the collapsed globule crystallizes. Due to slow crystallization kinetics, this transition may be undercooled and rather at $T_{\mathrm{g}} < T_{\mathrm{crys}}(\infty)$ the collapsed globule freezes in a glassy state. Since we assume that the transition lines vary linearly with the interaction volume λ^3, λ^3 rather than λ has been chosen as an abscissa variable.

a transition (that becomes a sharp thermodynamic first-order transition in the thermodynamic limit, $N \to \infty$) from coil to disk-like or toroidal structures, with strong bond-orientational order along the chain. More recently, it was found that even for fully flexible chains crystallization of polymers may preempt the collapse into a fluid globule [9–12]. Whether or not a fluid globule can exist depends on the interaction range λ of the attractive part of the interaction (figure 2), and this also has important consequences for the phase diagram of a polymer solution at finite N and nonzero monomer density ρ (figure 3). Of course, keeping N finite and taking rather the number of chains M to infinity is the traditional way to take the thermodynamic limit. For $\lambda > \lambda_t$ (figure 3, right part) the phase diagram qualitatively resembles that of a system of small molecules. The only peculiarity is that the critical point moves into the theta point at $\rho = 0$ if $N \to \infty$,

$$\Theta - T_C(N) \propto N^{-1/2}, \qquad \rho_c \propto N^{-1/2}. \qquad (3)$$

In equation (3), logarithmic corrections again are disregarded throughout.

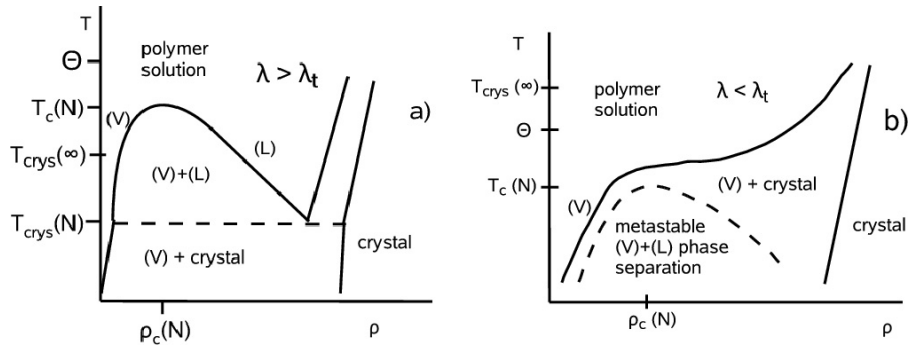

Figure 3. Schematic phase diagram of polymer solutions at fixed finite chain length N, as a function of temperature T and monomer density ρ, for $\lambda > \lambda_t$ (right part) and $\lambda < \lambda_t$ (left part). For $\lambda > \lambda_t$ one has $\Theta > T_{\rm crys}(\infty)$, and for large N the solution separates into a dilute solution of collapsed chains (corresponding qualitatively to the vapor (V) phase of a small molecule fluid) and a concentrated solution (corresponding to the liquid (L) phase). For $T < T_{\rm crys}(N)$ only vapor and crystal phases exist in thermal equilibrium. For $\lambda < \lambda_t$, however, $\Theta < T_{\rm crys}(\infty)$, and then a phase diagram with a 'swan neck'-topology may result, describing $V +$ crystal coexistence. $V + L$ phase separation may only occur as metastable states.

In the present work, we shall present evidence for figure 2, discussing Monte Carlo results [9–12] obtained for the bond fluctuation model [13, 14] using the Wang–Landau [15] algorithm. In section 2 we briefly recall the main features of this model and the simulation method. Section 3 then summarizes a few key results and draws an analogy between the phase behavior proposed in figure 3 and the (experimentally known) phase behavior of colloid–polymer mixtures [16]. Section 4 discusses briefly the collapse of semiflexible chains [7, 8, 17], while section 5 describes a recent extension discussing the competition between collapse of a polymer 'mushroom' (i.e., a chain endgrafted to a wall) and the adsorption transition [18–20]. Section 6 summarizes our conclusions.

2. Model and simulation method

We are not interested here in a chemically realistic description of particular polymers, but rather wish to qualitatively address the generic behavior. Therefore we use a simple coarse-grained model on the simple cubic lattice, the bond fluctuation model [13, 14]. In this model, one imagines that several chemical monomers along the chain backbone are integrated into a single effective bond, connecting two effective monomers. Each effective monomer is described by an elementary cube of the lattice. All 8 corner sites of the cube cannot be occupied by any other monomer, modeling thus excluded volume interactions. The bonds are not uniquely fixed in their length, but rather can take any of the vectors (measuring all lengths in units of the lattice spacing) $\{(\pm2, 0, 0); (\pm2, \pm1, 0); (\pm2, \pm1, \pm1); (\pm2, \pm2, \pm1); (\pm3, 0, 0); (\pm3, \pm1, 0);\}$, or permutations thereof. It turns out [13, 14] that this model can be simulated by Monte Carlo methods [21, 22] particularly efficiently, and the approach to the asymptotic behavior of long self-avoiding walks with increasing chain length N is particularly rapid [13, 14]. Each effective bond represents several chemical monomers, which due to multiple minima of the torsional potential for each bond give rise to many different states for a group of subsequent chemical monomers, allowing different choices of effective bonds is not only computationally convenient but also physically reasonable [22].

Temperature is introduced into the model by an attractive square well interaction of depth $\varepsilon(= 1)$ and range λ between all monomers, so that the Hamiltonian becomes

$$H = -\varepsilon N q, \tag{4}$$

where q is the number of neighbors per monomer, i.e. the number of other monomers within the interaction range λ. Two values of λ will be considered, $\lambda_1 = \sqrt{6}$ and $\lambda_2 = \sqrt{10}$. In order to describe variable chain stiffness, a bond potential can be introduced

$$U_{\rm bond}(\vartheta) = bT(\cos\vartheta - 1)^2, \tag{5}$$

ϑ being the angle between the directions of the adjacent bonds, and b the associate chain stiffness parameter. Normally we choose $b = 0$, however.

Since we shall consider (figure 2) the interplay between the formation of collapsed liquid globules and crystalline states, the choice of an underlying simple cubic lattice severely constrains the phenomena that can be described: only crystal structures commensurate with the underlying lattice can form. However, while no such constraint is present for off-lattice bead-spring models [22], using the latter models for the study of the present problem [23, 24] brings little advantages, since the states of very low energy are much harder to find (or even missed). Moreover, also the crystal structures of bead-spring chains are still far from chemical reality, and a study of collapse and crystallization of polymers using chemically realistic all-atom models is far beyond present computer resources. Thus we feel that the present model is a reasonable compromise, capturing the phenomena of interest qualitatively, though a direct mapping to experiment clearly is not possible.

The Monte Carlo method used applies 'random hopping', 'slithering snake' and 'pivot-like' moves [22], but we do not apply the Metropolis algorithm [21] but rather the Wang–Landau algorithm [15], to directly sample the energy density of

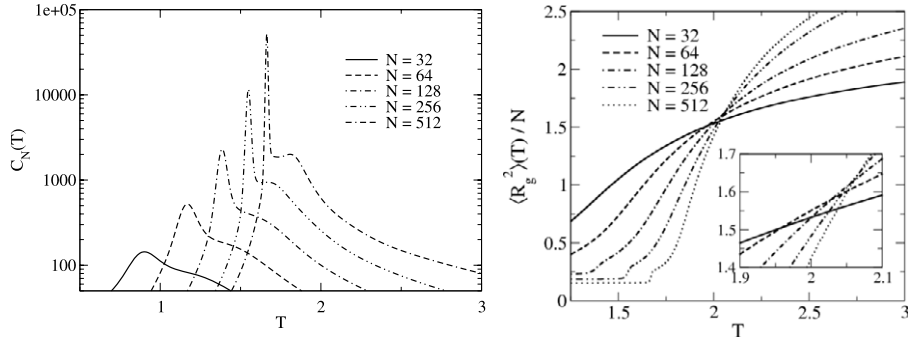

Figure 4. (a) Specific heat (on a log scale) plotted versus temperature for different chain length N as indicated, choosing the interaction range $\lambda = \lambda_1 = \sqrt{6}$. The uncertainty of the curves is below 2% as given by independent runs for the estimation of $g(E)$ at fixed N. From Rampf *et al* [9]. (b) Plot of $\langle R_g^2 \rangle_T / N$ versus T, for $\lambda = \lambda_1$ and different N. The inset shows a magnification of the region near the intersection points. Reproduced from [9] with permission. Copyright 2005 IOP Publishing Ltd.

states $g(E)$. I.e., the acceptance probability of a move from an old configuration (with energy $E_{\rm old}$) to a new one (with energy $E_{\rm new}$) is

$$\text{prob(old} \to \text{new)} = \min[1, g(E_{\rm old})/g(E_{\rm new})]. \qquad (6)$$

If $g(E)$ is known, equation (6) leads to a random walk through configuration space, and a flat histogram $H(E)$ counting how often different energies E are visited in the course of the sampling results. Although $g(E)$ in general is unknown, of course, one can build an iteration procedure on equation (6) [15]. Initially, one puts $g(E) = 1$ for all possible values of E, and $H(E) = 0$. Whenever E is reached, one replaces $g(E)$ by $fg(E)$ and $H(E)$ by $H(E) + 1$, where the factor f initially is arbitrarily chosen $f = e$ for the first round of iteration (from round to round the factor is decreased according to $f_{\rm new} = \sqrt{f_{\rm old}}$, until $f \to 1$. At each new round one starts with $H(E) = 0$, of course). An iteration round is stopped when the histogram $H(E)$ is sufficiently 'flat' (i.e., the smallest value in the histogram is at least 80% of the average value of the histogram entries). When $f \to 1$, the method fulfils detailed balance (with equation (6)).

From $g(E)$ one readily obtains the canonical partition function as well as all averages of interest

$$Z(T) = \sum_E g(E)\, \exp(-E/T), \qquad F = -T \ln Z, \qquad (7)$$

$$\langle E^k \rangle_T = \sum_E E^k\, g(E)\, \exp(-E/T)/Z(T), \quad k = 1, 2, 3, \ldots \qquad (8)$$

in particular the specific heat $C(T)$

$$C(T) = \left[\langle E^2 \rangle_T - \langle E \rangle_T^2 \right] / T^2. \qquad (9)$$

However, when $N = 512$ we already encounter a variation of $\ln g(E)$ from about -500 (for collapsed chains) to $+400$ (for swollen chains), and hence it is clear that the numerical effort increases rapidly with N. One can also sample structural quantities, such as $\langle R_g^2 \rangle_T$, though the statistical effort then is even larger, since one needs to record $R_g^2(X_E)$ in each configuration X_E belonging to the final histogram $H(E)$ for energy E,

$$\overline{R_g^2} = [g(E)]^{-1} \sum_{X_E} R_g^2(X_E) \approx [H(E)]^{-1} \sum_{X_E=1}^{H(E)} R_g^2(X_E) \qquad (10)$$

$$\left\langle R_g^2 \right\rangle_T = \sum_E g(E)\, \overline{R_g^2}\, \exp(-E/T)/Z(T). \qquad (11)$$

3. Collapse versus crystallization of flexible chains

From figure 4(a) one sees that the specific heats start to develop gradually a broad peak at rather high temperature, but on top of this broad peak a somewhat sharper feature grows on the low temperature side. This peak grows into a delta function as $N \to \infty$, and is connected with the crystallization transition of our model, as we shall see. The position of both peaks shift to higher temperature with increasing chain length.

Figure 4(b) presents the corresponding data for $\langle R_g^2 \rangle_T$. The standard recipe to locate the collapse transition is to plot $\langle R_g^2 \rangle_T / N$ versus T for several choices of N and try to locate Θ from the intersection point: we expect that in the swollen region (for $T > \Theta$) this ratio should increase with N, while in the collapsed region (for $T < \Theta$) this ratio should decrease with N. Only for $T = \Theta$ an unique intersection (persisting for $N \to \infty$) should exist. This expectation seems to work, when one chooses a plot with a very wide temperature range on the abscissa; but a closer look (inset of figure 4(b)) shows that there occurs rather a systematic finite chain length effect: each successive pair $(N, 2N)$ yields a slightly different estimate $T_\Theta(N)$, and these estimates increase with N systematically. It turns out that the extrapolation suggested from the standard theory of the collapse transition [2]

$$T_\Theta(N) = \Theta - a_1/\sqrt{N} \qquad (12)$$

works rather well (figure 5(a)). In equation (12), a_1 is a phenomenological constant. It is gratifying that equation (12) also works for the specific heat peak location, and although then a_1 is quite large, the extrapolations from $C(T)$ and $\langle R_g^2 \rangle_T / N$ are very well compatible with each other, namely

$$\Theta(\lambda_1) = 2.14 \pm 0.04, \qquad \Theta(\lambda_2) = 4.0 \pm 0.1. \qquad (13)$$

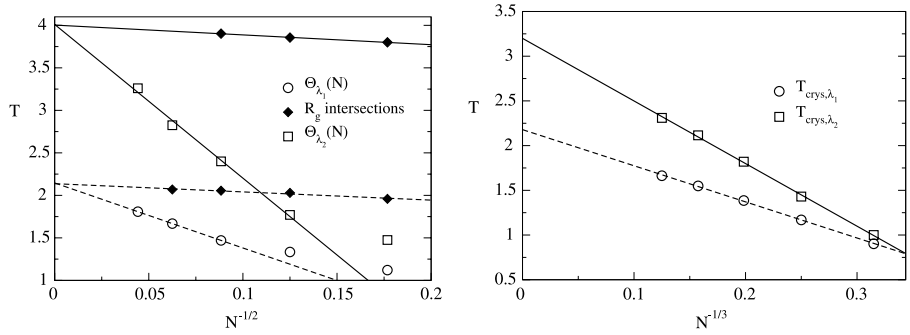

Figure 5. (a) Extrapolation of the location of the coil-globule transition located by the broad high-temperature peaks in the specific heat curves (figure 4(a)) for λ_1 (open circle) and λ_2 (open squares). The diamonds indicate intersection points in plots of $\langle R_g^2\rangle_T/N$ versus T for chains of length N and $2N$ (figure 4(b)). Note that $N^{-1/2}$ is used as abscissa, consistent with equation (12). From Paul *et al* [12].
(b) Extrapolation of the location of the liquid–solid transition, extracted from the sharp peak of $C(T)$ at low temperatures, versus $N^{-1/3}$. From Paul *et al* [12]. Copyright 2007, American Physical Society.

The liquid to solid transition is a first-order transition where the bulk free energy densities of the liquid and solid globules are identical. The surface excess free energies due to the free surfaces of the liquid and solid globules are not expected to also coincide, however: thus we expect a finite-size shift of the crystallization transition due to the relative difference in surface free energies

$$T_{\rm crys}(N) = T_{\rm crys}(\infty) - b_1/N^{1/3}, \qquad (14)$$

where b_1 is another phenomenological parameter. Figure 5(b) shows that our data are fit perfectly by equation (14), leading to

$$T_{\rm crys}(\lambda_1) = 2.18 \pm 0.01, \qquad T_{\rm crys}(\lambda_2) = 3.20 \pm 0.02. \quad (15)$$

Thus, for $\sqrt{10}$ we do have a broad temperature range where the fluid globule exists, $3.2 < T < 4.0$, while for $\lambda_1 = \sqrt{6}$ we do not: for $N \to \infty$ $T_{\rm crys}(\infty)$ seems to exceed Θ slightly! These findings hence provide clear evidence for the scenario proposed in figure 2, obviously λ_1 must be close to the value λ_t where the (tricritical) line of coil-globule transitions (for $N \to \infty$) hits the (first-order) crystallization transition curve in a (tricritical) endpoint.

Examining the configurations of the polymer for $T < T_{\rm crys}(N)$ one can check that the configurations dominating the low temperature phase indeed are crystals [9–11] rather than glass-like states. It is also interesting to study for finite N the liquid–solid coexistence (which occurs for $T = T_{\rm crys}(N)$ where the specific heat has its sharp maximum): considering the radial density profiles $\rho(r)$ of the globules [10], one finds that both in the liquid and in the solid state one can distinguish a 'bulk' region where the density is flat, $\rho(r) \approx \rho_{\rm liq}(N)$ and $\rho(r) \approx \rho_{\rm sol}(N)$, before $\rho(r)$ decays to zero in an interfacial region. While $\rho_{\rm sol}(N) \approx 1.0$ independent of N, for $\rho_{\rm liq}(N)$ a very different behavior is found: while $\rho_{\rm liq}(N \to \infty)$ for $\lambda = \lambda_2$ extrapolates towards a nonzero constant, as expected, for $\lambda = \lambda_1$ it seems that $\rho_{\rm liq}(N \to \infty)$ vanishes, since the data can be fitted by the (empirical) power law, $\rho_{\rm liq} = 1.2\, N^{-0.153}$. If $T_{\rm crys}(\infty) = \Theta$, however, a simple geometric construction readily yields $\rho_{\rm liq} \propto N^{-1/3}$, however, since the liquid branch of the vapor–liquid coexistence curve for $N \to \infty$ tends to a straight line ending at $T = \Theta$ at the ordinate axis in figure 3. Thus, we do not have a theoretical explanation for the (effective?) exponent 0.153 observed in the simulation.

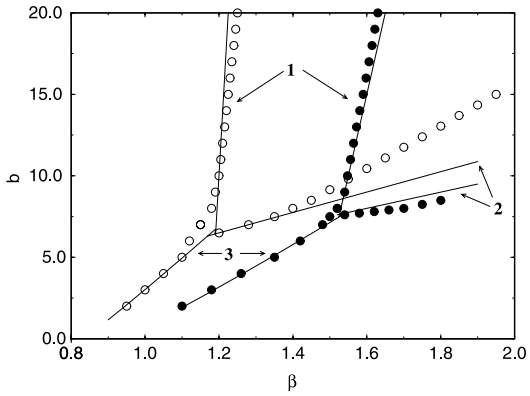

Figure 6. Theoretical (solid lines) and simulational (circles) diagrams of states for semiflexible chains, described by the bond fluctuation model with $N = 80$ (open symbols) or $N = 40$ (full symbols), in the plane of variables b (stiffness potential strength, compare equation (5)) and $\beta = 1/T$. Solid lines are given by the formulas: (1) $b = a_1 + a_2\,\beta\,N^2$; (2) $b = a_1' + a_2'\,\beta\,N^{1/3}$; (3) $b = a_1'' + a_2''\,\beta^{4/3}\,N^{2/3}$, where $a_1, a_1', a_1'', a_2, a_2', a_2''$ are parameters adjusted from the best fits of the simulation data to these formulas. From Stukan *et al* [8]. Copyright 2003, American Institute of Physics.

As a final remark of this section, we point out the similarity of the homopolymer solution phase diagrams proposed in figure 3 with the phase diagrams known for colloid–polymer mixtures [16, 25, 26]. Representing colloids as hard spheres of radius R_c which may neither overlap each other nor the polymers, while the latter may overlap each other with zero or little ($\approx 2T$) energy cost, the polymers cause a depletion attraction among the colloids, which has a range of R_g, and hence may be much smaller than R_c, if a suitable size ratio R_g/R_c between polymers and colloids is chosen. For the resulting entropy-driven liquid–vapor type phase separation into a polymer-rich (the 'vapor') and a colloid-rich phase (the 'liquid') the polymer fugacity plays the role of inverse temperature, when we refer to the phase diagram, figure 3. It is established both from experiment [16] and from simulation [26] that for small enough R_g/R_c this

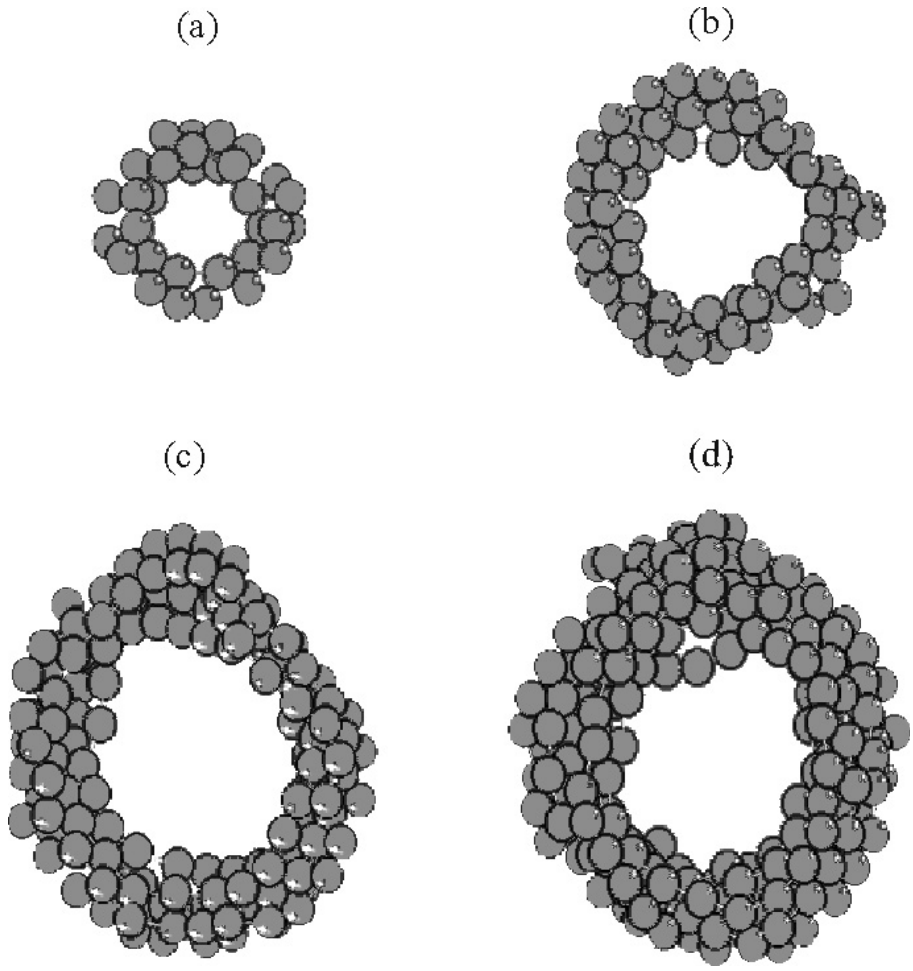

Figure 7. Snapshot pictures of toroidal structures for different chain length: $N = 40$ (a), 80 (b), 160 (c) and 240 (d). All data refer to a stiffness potential strength $b = 15$, but different inverse temperatures $\beta = 1.6$ (a), 1.3 (b), 1.1 (c) and 1.0 (d). The (cubic) monomers of the bond fluctuation model were drawn here as shaded spheres, and the bonds connecting them are not shown. From Stukan *et al* [8]. Copyright 2003, American Institute of Physics.

vapor–liquid type phase separation becomes unstable, since the critical point decreases more strongly with decreasing R_g/R_c than the triple point in figure 3, and ultimately the 'swan neck' topology of the phase diagram results. Defining a scaled width $R = \lambda/\sigma - 1$ of the square well attraction (σ is the range of the hard core repulsion), Noro and Frenkel [26] found that for $R \leqslant 0.14$ the vapor–liquid criticality becomes unstable. We hence suggest that a related phenomenon should be observable in polymer solutions, when one has flexible chains made from rather 'bulky' monomers, so that the range of the monomer–monomer-attractions becomes small enough in comparison with the range of the excluded volume interaction.

4. Collapse of semiflexible chains

While in the previous section fully flexible chains were considered, i.e. no bond angle potential such as equation (5) was applied, we now briefly discuss the effect of increasing chain stiffness on the collapse transition [6–8, 17]. This problem has been studied by standard Monte Carlo methods [7, 8] (applying the Metropolis algorithm [21]), and we here only briefly recall the main findings, for the sake of comparison to the results presented in the previous transition: figure 6 shows that with increasing chain stiffness the coil-globule transition is shifted to lower temperature, until it also ends at another transition line (of first-order character) where disk-like globules or toroidal structures are formed (figure 7). These structures are not as disordered as the spherical collapsed globules are, but rather exhibit a pronounced bond-orientational order, although a full crystalline order is not present. It is possible, however, that such states are only precursors for larger rodlike or spherical globules that exhibit liquid-crystalline order. Due to the potential, equation (5), in solutions of polymers of finite chain length but nonzero monomer concentration indeed a phase separation where a solution with nematic order appears as the high density phase is known to occur. Thus, approaching the thermodynamic limit at $\rho = 0$ for a single chain, $N \to \infty$, it is natural to expect that states of a single chain which exhibit also nematic order should occur.

5. Polymers in contact with a wall: collapse versus adsorption

When a dilute polymer solution under bad solvent conditions is exposed to an attractive wall, one can again discuss the

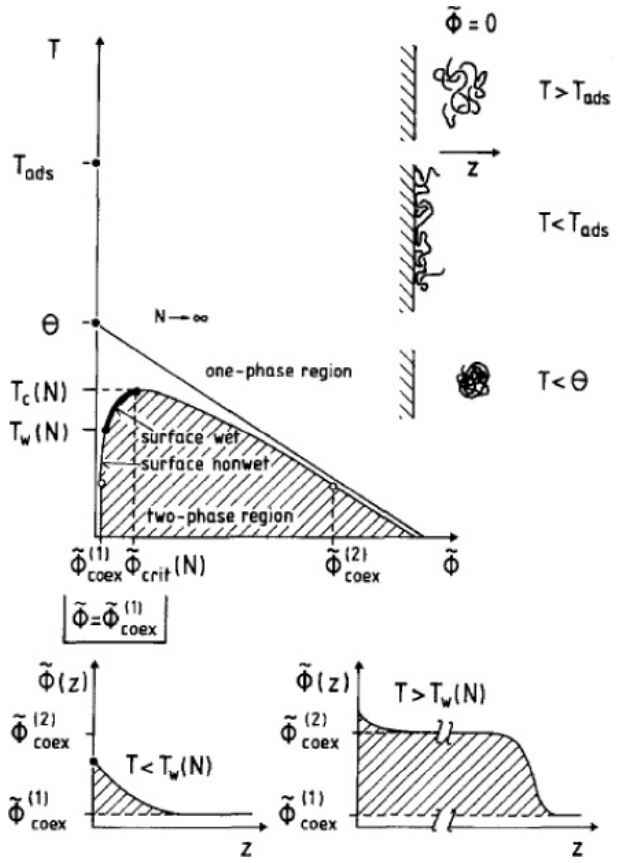

Figure 8. Schematic phase diagram of a polymer solution in semi-infinite space ($z > 0$) with one attractive wall, plotted as a function of temperature T and volume fraction ϕ taken by the monomers (upper part, left). For $T < T_c(N)$ two-phase coexistence occurs (shaded). For $\phi = \phi^{(1)}_{coex}$ and $T_w(N) < T < T_c(N)$, formation of a wetting layer at the wall occurs (see the schematic volume fraction profile $\phi(z)$ versus z in the lower right part; the profile in the left part refers to a non-wet wall, as it occurs for $T < T_w(N)$). In addition, it is assumed that for $N \to \infty$ at $T = T_a$ in the good solvent regime ($T_a > \Theta$) an adsorption transition occurs (cf text). Adapted from Milchev and Binder [30].

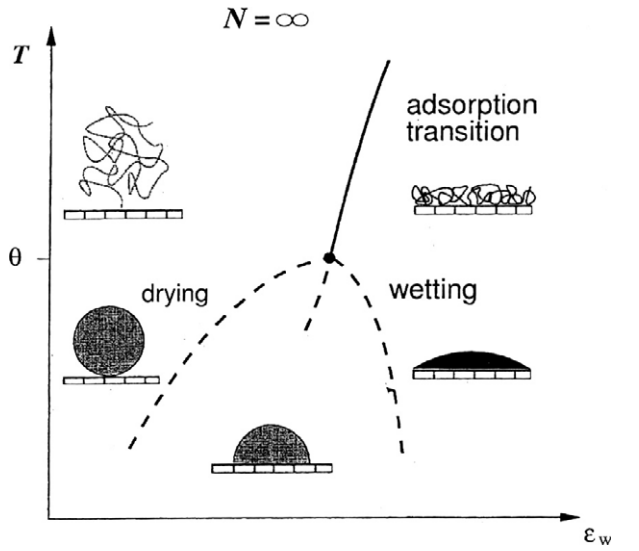

Figure 9. Phase diagram of a polymer mushroom (flexible polymer anchoring with one end at the flat attractive surface) in the limit $N \to \infty$ as a function of temperature T and the monomer–wall attraction ε_w. States shown are a swollen mushroom ($T > \Theta$, left), swollen pancake ($T > \Theta$, right), a collapsed globule forming a spherical droplet just touching the wall in the anchor point ($T < \Theta$, left), a sphere-cap shaped collapsed globule in the regime in between drying and wetting transitions (broken curves), and a collapsed pancake ($T < \Theta$, right). Adapted from Metzger *et al* [18].

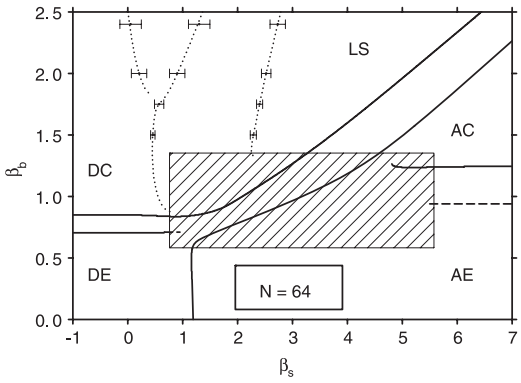

Figure 10. Diagram of states of a polymer mushroom with $N = 64$ using the bond fluctuation model, in the plane of parameters $\beta_b = \varepsilon/k_BT$ and $\beta_s = \varepsilon_w/k_BT$ (the energy ε_w is won by monomers in the planes $z = 1$ and 2, respectively, while no monomer can occupy lattice sites for $z \leqslant 0$). States shown are 'desorbed collapsed' (DC), 'desorbed expanded' (DE), 'adsorbed expanded' (AE), 'adsorbed collapsed' (AC) and 'layered structures' (LS). Boundaries between these states (lines) represent maxima in the fluctuations of bead contacts or monomer–surface contacts, respectively. The shaded rectangle shows a region where the different states are no longer clearly distinguishable. For further explanations see the text. From Luettmer-Strathmann *et al* [19]. Copyright 2008, American Institute of Physics.

competition between wall-monomer and monomer–monomer attractions considering two ways of taking the thermodynamic limit: from the point of view of the liquid–vapor phase separation of the solution at finite N (but taking the number of chains M and hence the system volume to infinite) we expect near the bulk critical point a wetting transition of the wall (figure 8, middle part): at low temperatures the wall is non-wet, there is only a modest enhancement of the polymer concentration close to the wall (figure 8, lower left part). Above the wetting transition, a thick layer of the liquid phase intrudes near the wall (figure 8, lower right part).

From the point of view of single chain transitions in the limit of infinite chain length, however, there is a competition between the adsorption transition from a coil to a quasi-two-dimensional 'pancake' attracted to the surface [27–31] with collapse in the bulk (figure 8, upper middle part).

Of course, it is again tempting to speculate how the two scenarios to approach the thermodynamic limit are related. Figure 9 shows such a speculation [31]: while in the good solvent regime the non-adsorbed 'mushroom' (endgrafted flexible macromolecule) stretches away from the wall, it forms a (semidilute) 'pancake' [27–29] when the adsorption transition for $T > \Theta$ has occurred. While this transition has been carefully investigated (e.g. [29, 31]), much less is known for $T < \Theta$. Figure 9 disregards crystallization, and suggests that for $N \to \infty$ the wetting and drying transitions merge at $T = \Theta$ at the endpoint of the adsorption transition

line. In between drying and wetting transition lines, 'surface-attached globules' are expected, which were already suggested in a different context [32].

The actual phase diagram of polymer chains that are endgrafted at attractive surfaces and described by the bond fluctuation model on the simple cubic lattice is still the subject of ongoing work [19, 33]. Figure 10 presents a 'surface phase diagram' of a polymer mushroom for $N = 64$. We use quotation marks here to emphasize that a true phase diagram can only result when the limit $N \to \infty$ is taken, of course, and so the transitions between the different states are gradual (no singularities occur along the lines drawn in figure 10), and sometimes the transitions are so smeared out that they cannot be identified any longer (shaded region of the phase diagram). Note also that no clear evidence for the 'surface-attached globules' is found—rather the wall stabilizes layered crystalline structures (double layers, triple layers, etc) in a significant range of the phase diagram. Note, however, that figure 10 refers to the short range case $\lambda_1 = \sqrt{6}$ of the monomer–monomer attraction only. But this study did require an extension of the Wang–Landau technique [15] to sample two-dimensional histogram $H(E_b, E_w)$ of both bulk (E_b) and surface (E_w) contributions to the total energy of the chains.

6. Conclusions

In this paper Monte Carlo simulations of conformational changes of single chains were described. Such transitions can be induced by variation of solvent quality or chain stiffness in the bulk, and by interaction forces with walls when one considers polymers endgrafted on surfaces. It has been shown that a very rich phase behavior emerges, even in the framework of a very idealized and simplified model, the bond fluctuation model on the simple cubic lattice. We have payed particular attention to the fact that the range of attractive interactions is a very important control parameter for polymers, both with respect to the single chain behavior, and with respect to the phase diagram of polymer solutions at finite monomer concentration. States with crystalline order (and liquid-crystalline order, if stiff rather than flexible polymers are considered) play a role, both in the bulk, and when adsorption at surfaces is considered. It is an intriguing question to clarify whether polymers exist which are close in behavior to the present model rather than the standard model for lamellar crystallization [34, 35].

There are many directions in which the present studies could be extended (e.g. copolymers of various architectures, off-lattice models, adsorption on structured substrates, etc). It is hoped that the present study will stimulate such work, and last not least guide experiment to search for some of the predicted phenomena.

Acknowledgments

This research was supported in part by the Deutsche Forschungsgemeinschaft, SFB 625/A3, and grant No 436 RUS 113/223.

References

[1] de Gennes P-G 1979 *Scaling Concepts in Polymer Physics* (Ithaca, NY: Carnill University Press)
[2] Grosberg A Y and Khokhlov A R 1994 *Statistical Physics of Macromolecules* (New York: AIP)
[3] Des Cloizeaux J and Jannink G 1990 *Polymers in Solution: Their Modeling and Structure* (Oxford: Clarendon)
[4] Wu C and Wang X 1998 *Phys. Rev. Lett.* **80** 4092
[5] Grassberger P 1997 *Phys. Rev.* E **56** 3682
[6] Grosberg A Y and Khokhlov A R 1981 *Adv. Polym. Sci.* **41** 53
[7] Ivanov V A, Paul W and Binder K 1998 *J. Chem. Phys.* **109** 5659
[8] Stukan M R, Ivanov V A, Grosberg A Y, Paul W and Binder K 2003 *J. Chem. Phys.* **118** 3392
[9] Rampf F, Paul W and Binder K 2005 *Europhys. Lett.* **70** 628
[10] Rampf F, Binder K and Paul W 2006 *J. Polym. Sci.* B **44** 2542
[11] Paul W, Rampf F, Strauch T and Binder K 2007 *Macromol. Symp.* **252** 11
[12] Paul W, Strauch T, Rampf F and Binder K 2007 *Phys. Rev.* E **75** 060801[R]
[13] Carmesin I and Kremer K 1988 *Macromolecules* **21** 2819
[14] Paul W, Binder K, Heermann D W and Kremer K 1991 *J. Physique* II **1** 37
[15] Wang F and Landau D P 2001 *Phys. Rev.* E **64** 056101
[16] Ilett S M, Orrock A, Poon W C-K and Pusey P N 1995 *Phys. Rev.* E **51** 1344
[17] Martemyanova J A, Stukan M R, Ivanov V A, Mueller M, Paul W and Binder K 2005 *J. Chem. Phys.* **122** 174907
[18] Metzger S, Mueller M, Binder K and Baschnagel J 2003 *J. Chem. Phys.* **118** 8489
[19] Luettmer-Strathmann J, Rampf F, Paul W and Binder K 2008 *J. Chem. Phys.* **128** 064903
[20] Ivanov V A, Martemyanova J A, Mueller M, Paul W and Binder K 2008 *J. Chem. Phys.* B at press
[21] Landau D P and Binder K 2005 *A Guide to Monte Carlo Simulations in Statistical Physics* 2nd edn (Cambridge: Cambridge University Press)
[22] Binder K (ed) 1995 *Monte Carlo and Molecular Dynamics Simulations in Polymer Science* (New York: Oxford University Press)
[23] Parrons D F and Williams D R M 2006 *Phys. Rev.* E **74** 041804
[24] Seaton D T, Mitchell S J and Landau D P 2008 *Braz. J. Phys.* **38** 48
[25] Lekkerkerker H N, Poon W K-C, Pusey P N, Stroobants A and Warren P B 1992 *Europhys. Lett.* **20** 559
[26] Noro M G and Frenkel D 2000 *J. Chem. Phys.* **113** 2941
[27] de Gennes P-G 1976 *J. Physique* **37** 1445
[28] de Gennes P-G 1980 *Macromolecules* **13** 1069
[29] Eisenriegler E, Kremer K and Binder K 1982 *J. Chem. Phys.* **77** 6296
[30] Milchev A and Binder K 1996 *J. Comput.-Aided Mater. Des.* **2** 167
[31] Metzger S, Mueller M, Binder K and Baschnagel J 2002 *Macromol. Theory Simul.* **11** 985
[32] Rajesh R, Dhar D, Giri D, Kumar S and Singh Y 2002 *Phys. Rev.* E **65** 056124
[33] Luettmer-Strathmann J, Rampf F, Paul W and Binder K 2008 in preparation
[34] Sommer J-U and Reiter G (ed) 2003 *Polymer Crystallization: Observation Concepts and Interpretation* (Berlin: Springer)
[35] Hu W B and Frenkel D 2006 *J. Phys. Chem.* B **110** 3734